Molecular dynamics of unstable motions and capillary instability in liquid nanojets

Yong Seok Choi, Sung Jin Kim,* and Moon-Uhn Kim
Department of Mechanical Engineering,Korea Advanced Institute of Science and Technology, Daejeon, 305-701, South Korea
(Received 28 April 2005; revised manuscript received 30 August 2005; published 30 January 2006)

We present an investigation of the capillary instability of nanometer-sized surface-tension-driven flow using molecular dynamics (MD) simulations with Lennard-Jones fluid. Unstable motions of a liquid nanojet are successfully simulated and it is found that the thermal fluctuation, which is significant in a nanoscale system, is the most important factor for various breakup scenarios of a nanojet. The nanojet diameter at the nozzle outlet is varied to show the effect of size on the rupture phenomena and the formation of small droplets. Numerical results for the rupture time and the growth rate of spherical droplets are compared with those of various classical linear instability theories. Even though the MD simulation results for the growth rate of the droplets are close to those predicted by the classical instability theories, the former are shown to be independent of the wave number unlike the latter. Therefore, the classical continuum-based theories may not be applicable to studying the instability of nanoscale systems.

DOI: 10.1103/PhysRevE.73.016309 PACS number(s): 47.20.Dr

I. INTRODUCTION

Liquid jets have long been of great interest due to their particular characteristics involving unstable motions and rupture phenomena which provide fundamental ideas for a wide range of engineering applications, such as spraying, mixing, fuel injection, and ink-jet printing. Pioneering works on liquid jet behaviors were performed by Lord Rayleigh [1] who noticed that surface tension and inertia are the source of instability. Rayleigh found that there exists a fastest growing mode of disturbance and derived the dispersion relation between the dimensionless wave number and the growth rate of disturbance for inviscid incompressible liquid. His dispersion relation is in good agreement with his own experimental results. After Rayleigh's work, several theoretical and experimental studies had been conducted on liquid jet instability. Chandrasekhar [2] took the viscosity effect into account by solving the full Navier-Stokes equations. Goedde and Yuen [3] directly measured the growth rate of disturbance for the liquid jet by imposing external vibration and found that experimental results agreed well with the linearized analysis of Rayleigh [1] and Chandrasekhar [2].

When liquid-jet rupture phenomena occur on a nanometer scale, it is questionable whether an approximation based on the continuum theories stated above is still valid [4]. Since nanoscale liquid jets, or nanojets, are expected to be used in fabricating nanostructures or for extremely small-scale pattern transfer on silicon chips, it is necessary to have an accurate understanding of unstable motions and rupture phenomena involving nanojets. Previous works on rupture phenomena have shown that the continuum equations are still relevant in nanoscale systems. Koplik and Banavar [5] studied the instability of a nanoscale liquid thread using MD simulation and concluded that the simulation results were in close agreement with the continuum calculations. Kawano [6] also investigated rupture phenomena in a relatively long liquid thread using MD simulation and found that the numerical results for the rupture time and the wave number agreed quantitatively well with the linear instability theory. It should be noted, however, that their simulation models are limited to an initially quiescent liquid thread, which is not emanating but intrinsically rearranges itself into droplets or smaller liquid threads. Also, considering that MD simulation results of a time-dependent liquid flow with a free surface are very sensitive to initial velocities, we cannot generalize the results of previous researchers on liquid threads [5,6]. Even though they claim that the linear instability theory is still applicable to the nanoscale liquid flow with a free surface, they did not provide sufficient simulation cases with many different initial velocities. Recently, Moseler and Landman [7] reported atomistic MD simulation results for liquid nanojet formation and instability. They found that the presence of thermally triggered fluctuations produced a significant effect on the breakup characteristics of nanojets and presented a modified lubrication equation to relate it with an atomic description. They concentrated only on the application of the lubrication equation to a nanometer scale jet and did not investigate the relation between the wavelength and the growth rate of the disturbance of the nanojet.

In this paper, we consider a liquid nanojet made of 10 000 Lennard-Jones molecules and check the validity of the classical linear instability theories so as to determine whether they are applicable to the rupture phenomena of a nanojet using various simulation conditions. First, we present hydrodynamic behaviors of a liquid jet discharging from a nozzle with an orifice shape. With various diameters at the nozzle outlet and various initial conditions, we present numerical results for the rupture time of the nanojet and compare them with those based on a macroscopic viewpoint. Finally, we present the distributions of the growth rate of the disturbance as a function of the wave number and then compare them with the analysis of Rayleigh [1] and Chandrasekhar [2].

*Corresponding author.
Electronic address: sungjinkim@kaist.ac.kr

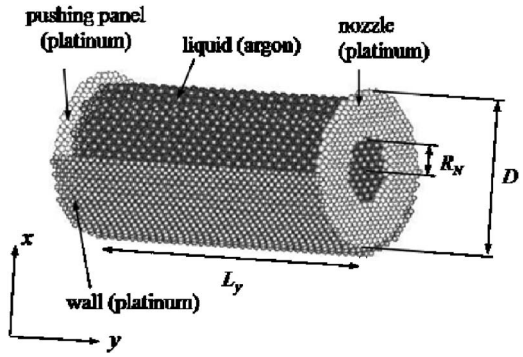

FIG. 1. Simulation geometry of cylinder for nanojet process. Diameter $D^*=21$ and length $L_y^*=45$. Nozzle radius R_N^* is varied from 4.0405 to 5.1949 with an increment of 0.5772. Here the asterisk means reduced units. At first nozzle hole is closed and liquid atoms interact with wall atoms freely to achieve the thermal equilibrium.

II. MOLECULAR DYNAMICS SIMULATIONS

To provide atomic information on liquid nanojet processing, we used the molecular dynamics simulation method. The geometry for the simulation is shown in Fig. 1. The cylinder-shaped solid wall is made of 10 348 platinum atoms and the fluid is 10 000 argon atoms in liquid phase. A pushing panel is also made of platinum atoms and thrusts fluid atoms into the nozzle with the constant velocity. The liquid atoms are placed initially in a lattice structure of cylindrical shape that is surrounded by solid wall atoms and equilibrated for 70 000 time steps to achieve the equilibrium state before the production period is performed. The equilibration period allows liquid to reach the desired temperature.

The interatomic potential function among the liquid atoms is the well-known Lennard-Jones 12-6 potential, which is expressed as

$$\phi(r_{ij}) = 4\varepsilon\left[\left(\frac{\sigma}{r_{ij}}\right)^{12} - \left(\frac{\sigma}{r_{ij}}\right)^{6}\right], \quad (1)$$

where ε and σ are the energy and the length parameters, respectively, and r_{ij} is the interatomic distance between atoms i and j. For the argon, the following parameters are used: $\sigma=\sigma_{liq}=0.34$ nm, $\varepsilon=\varepsilon_{liq}=1.66\times10^{-21}$ J, mass $m=66.9\times10^{-27}$ kg, and time $\tau=\sqrt{m\sigma^2/\varepsilon}=2.16\times10^{-12}$ sec. For proper scaling during the simulations, calculations are performed in reduced units. In particular, we defined the reduced quantities as follows: the reduced temperature $T^*=k_BT/\varepsilon$, the reduced length $r^*=r/\sigma$, the reduced density $\rho^*=\rho\sigma^3/m$, the reduced velocity $v^*=v\sqrt{m/\varepsilon}$, the reduced viscosity $\eta^*=\eta\sigma^2\sqrt{1/m\varepsilon}$, and the reduced surface tension $\gamma^*=\gamma\sigma^2/\varepsilon$, where k_B is the Boltzmann constant. The platinum solid atoms are dangled to their nominated lattice sites by a spring force with tethering potential [8]. The interaction force between the solid molecules is also described by Eq. (1) with $\sigma=\sigma_{sol}=0.254$ nm and $\varepsilon=\varepsilon_{sol}=1.09\times10^{-19}$ J corresponding to the platinum potential parameter and the energy parameter, respectively. The density of solid atoms is set to be 21 343 kg/m^3. For the solid-liquid interaction, we have followed Nagayama and Cheng's suggestions [9], where the modified Lennard-Jones potential is used as

$$\phi(r_{ij}) = 4\alpha\sqrt{\varepsilon_{liq}\varepsilon_{sol}}\left[\left(\frac{\sigma_{sol-liq}}{r_{ij}}\right)^{12} - \beta\left(\frac{\sigma_{sol-liq}}{r_{ij}}\right)^{6}\right], \quad (2)$$

where $\sigma_{sol-liq}=(\sigma_{sol}+\sigma_{liq})/2$ is based on the Lorentz-Berthelot rule. In Eq. (2), α and β are the hydrophilic and hydrophobic interaction factors, respectively. As α and β increase, liquid atoms distribute in an orderly fashion near the solid interface due to strong solid-liquid interaction. On the other hand, small values of α and β induce a hydrophobic phenomenon with a weak solid-liquid interaction which reduces interfacial resistance. In this study, to promote the liquid injection through a nozzle, we have chosen the small values of interaction strength: $\alpha=0.123$ and $\beta=0.1$.

To reduce the computation time, we performed all simulations with a cutoff distance $r_c=3.0\sigma$ and used the neighbor list method, which allows the time required to examine all pair separations to be proportional to the number of all atoms N instead of N^2. The equations of motion were solved by the leap-frog integration algorithm with a time step of $\Delta t=0.005\tau$. The solid wall temperature is kept to $T_{sol}^*=1.0$ by the use of Gaussian thermostat equations of motion [10]. The equilibration time is enough to reach the thermal equilibrium between the wall and the liquid. For the initial conditions, many different sets of random velocities corresponding to the same temperature were extracted from the Maxwell-Boltzmann distribution. This is simply achieved by choosing any seed values for the c or FORTRAN compiler's random number generator [5].

III. RESULTS AND DISCUSSION

The liquid nanojet is ejected through various outlet diameters of a nozzle into a vacuum by pushing the panel with the constant velocity of $v_p^*=0.2$. Since we are considering the hydrophobic surface between the liquid and the wall atoms, jets initially maintain the cylindrical shape after they issue from the nozzle, which is preferable in simulating breakup phenomena. Then they decay spontaneously into several drops, small liquid threads, or satellite drops due to the surface tension. Simulation results for different diameters at the nozzle outlet are presented in Fig. 2. Three pictures on the left side describe the instant that first ruptures have taken place. Pictures on the right side are those of the final time step. As can be seen in Fig. 2, liquid nanojets have various breakup points and rupture times t_R^* depending on the nozzle radius without any external disturbances. In addition, the wavelength λ^*, the average distance between drops or liquid threads, tends to decrease with the reduction of nozzle radius.

It should be noted that final jet shapes are very sensitive to the initial conditions. Since we cannot neglect the thermal fluctuation that is an intrinsic property of the nanoscale system [5], each of the different thermodynamic systems may have their own significance. In the molecular dynamics simulation method, initial conditions such as the molecular positions, velocities, accelerations, and thermodynamic

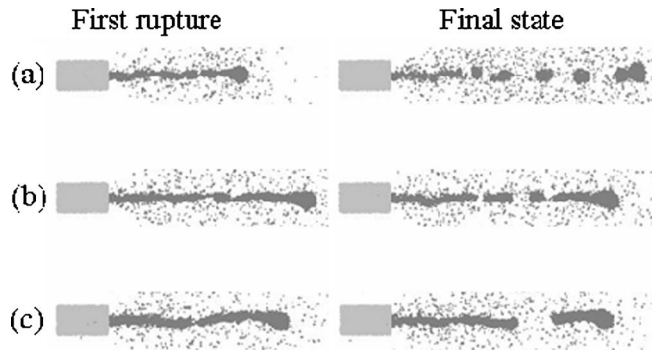

FIG. 2. Decaying nanojet behaviors for different radii of nozzle outlet. (a) $R_N^*=4.0405$, $t_R^*=92$, and $\lambda^*=33$; (b) $R_N^*=4.6177$, $t_R^*=137$, and $\lambda^*=42.6$; (c) $R_N^*=5.1949$, $t_R^*=121$, and $\lambda^*=83.5$.

states are usually given. All simulations start with the same initial conditions except for molecular velocities. The molecular velocities are randomly drawn from the Maxwell-Boltzmann distribution, which is defined in terms of the initially given temperature T^*. Different sets of velocities of the same distribution are selected according to the seed values in the random number generator. For the various seed values, jet breakup scenarios are shown in Fig. 3. Nonaxisymmetric neck shapes are shown for all simulation cases. The breakup length, the wavelength, and the formation of drops or liquid threads are shown to be randomly distributed. This means that simulation size in this study is not large enough to neglect molecular thermal fluctuation, which affects the simulation results in detail. First rupture times t_R^* for all simulation cases are plotted in Fig. 4. Simulation data are presented in reduced units. Note that the abscissa is the equimolar jet radius r_{eq}^*, which is defined as the point for which the radius becomes the average value of the liquid and vapor densities. For the same jet diameter, the rupture time has a wide range of distribution. As the jet radius increases, however, there is a tendency of increase in the rupture time. This is also the case for macroscale systems. That is, the time scale t_R is given by a balance of the surface tension force and the inertia force

$$t_R = \left(\frac{\rho r_{eq}^3}{\gamma}\right)^{1/2}, \tag{3}$$

where γ is the surface tension. Using the relation $t_R \sim r_{eq}^{3/2}$, the least-squares-fitted curve is shown in Fig. 4. Kawano [6]

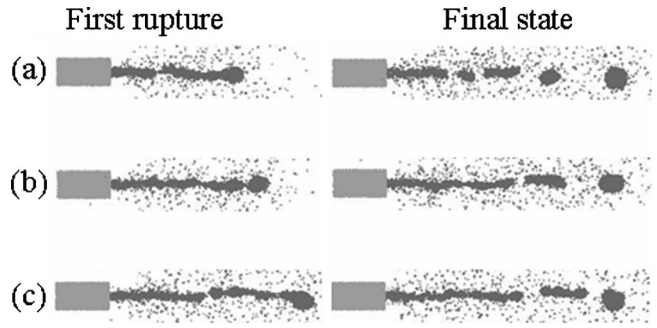

FIG. 3. Various jet shapes for different seed values at $R_N^*=4.6177$. (a) Seed value=13; (b) Seed value=15; (c) Seed value=17.

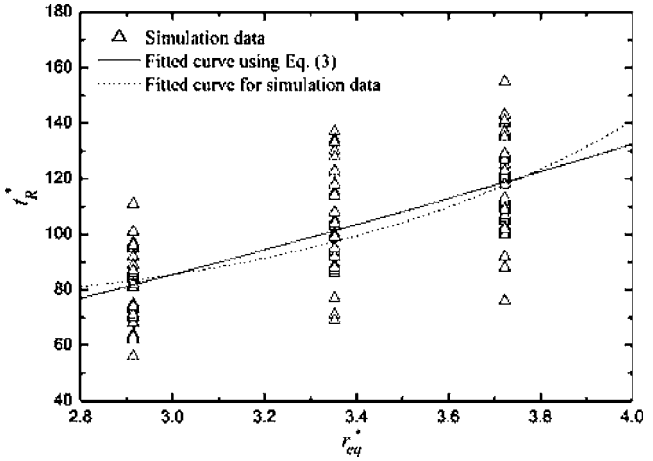

FIG. 4. First rupture times of the nanojet as a function of equimolar jet radius.

obtained similar simulation results for the rupture time. Even though the 3/2 power dependence is generally true for large scale jets, Moseler and Landman [7] claimed that there might be significant deviation from this dependence for nanojets. Hence, we have added in this figure another curve which fits simulation data. Its relation is $t_R \sim r_{eq}^{5.67}$.

A. Density, velocity, and temperature profiles across the nozzle

To see how the hydrodynamic properties such as density, streaming velocity, and temperature evolve across the nozzle, we have monitored the changes of these physical quantities. We confined the calculation domain to the distance of ten reduced units from the nozzle on both sides. We also divided the cylindrical liquid nanojet along the radial direction into a number of cylindrical shells. Thus, the hydrodynamic properties are computed as an average evaluated at the midpoint of the shell. This method is frequently called the slab method. To get a fine resolution in calculating the profile, a total of 51 shells are used for all simulation cases. The averaging time is long enough to contain a sufficiently large number of atoms in each shell.

The liquid density profiles are shown in Fig. 5. Here r^* is the radial distance from the center of the nozzle. To show how the hydrodynamic features change as the liquid goes through the nozzle, we divided the calculation domain into two regions. Inside the nozzle, the liquid density is always lager than the initially given value. As the nozzle diameter becomes large, the liquid density drops. This situation is the opposite outside the nozzle. Near the wall atoms the layering effect is found, which means the formation of liquid layers adjacent to the wall. The layered position is such that the most probable location of a liquid atom is at a fcc lattice site. The density attains its maximum value near the walls and becomes weaker toward the center of the nozzle. After the liquid passes through the nozzle, the density profiles rapidly approach the constant values of the liquid density ρ_{liq}^* as r^* decreases and of the vapor density ρ_{vap}^* as r^* becomes large. As stated above, we can define the equimolar jet radius r_{eq}^* or the interfacial position between the condensed liquid and the

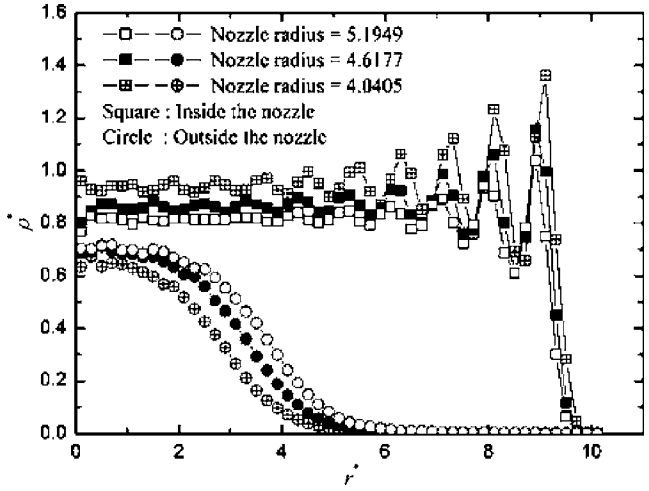

FIG. 5. Liquid density profiles across the nozzle. Calculation domain is divided into inside and outside regions.

vapor from Fig. 5 as the point at which the density is $(\rho^*_{liq}+\rho^*_{vap})/2$. The approximation adopted in this definition may be crucial to the calculation of the surface tension if we want to use the surface energy notion of Gibbs. We determined the surface tension differently based on a recent study on the liquid-vapor interface [11], which shows that we need the density distribution without having to know the interface position for calculating the surface tension.

The axial velocity profiles of the jet are shown in Fig. 6. To improve the statistical accuracy, we averaged the simulation data over various initial conditions using different seed values for a fixed nozzle radius. Inside the nozzle, the velocity profiles seem to decrease linearly toward the wall. We have shown the enlarged velocity profiles near the wall in the inset of Fig. 6. Due to a hydrophobic wall, velocity slips near the wall as expected. Regardless of the diameter at the nozzle outlet, all of the velocity profiles inside the nozzle are nearly the same. At the nozzle exit, velocities are increasingly accelerated to about four to six times higher than those inside the nozzle. It is found that the flow field of ejected jets is like plug flow, and this agrees well with the previous work [7].

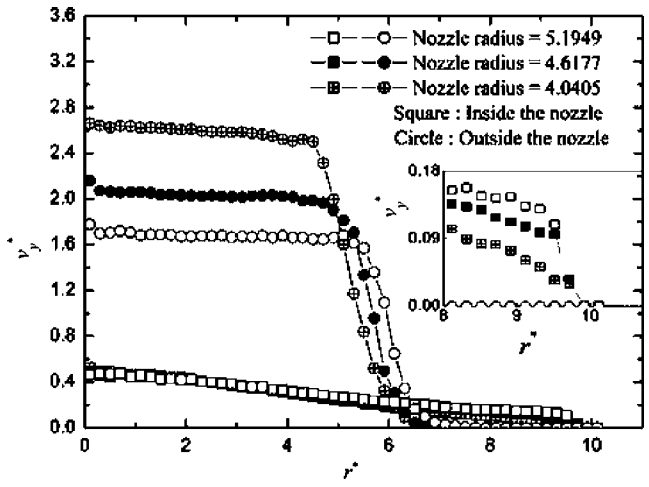

FIG. 6. Streaming axial velocity profiles of the jet.

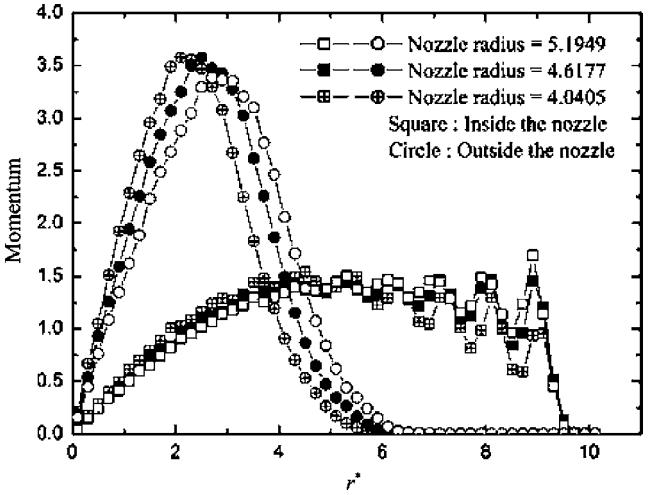

FIG. 7. Y-direction momentum profiles of the jet.

The y-directional momentum profiles are constructed using Figs. 5 and 6 and shown in Fig. 7. It is found that the y-directional momentum is conserved for the nanojet of the same nozzle radius.

The time-averaged temperature distributions inside the jet are calculated and shown in Fig. 8. Since we are interested in the hydrodynamic behavior of the jet only, the liquid temperature inside the nozzle was not calculated. It may be a matter of course that the jet temperature is not related to the nozzle radius macroscopically. The simulation results also show that the jet temperature almost does not vary with three cases of the nozzle radius. Since the emanating jet is evaporating to the vacuum, the fluid temperature decreases in the radial direction from its maximum temperature at the center. We can determine the effective temperature of the jet using the equimolar jet radius r^*_{eq} calculated by the density profiles. It is estimated to be $T^*_{jet}\cong 0.8$ for all three cases. Then we can calculate the temperature-dependent liquid properties, such as viscosity and surface tension by using T^*_{jet}. In Fig. 8, no data are available for temperature profiles near the center of the nozzle. This is because the calculation domain located

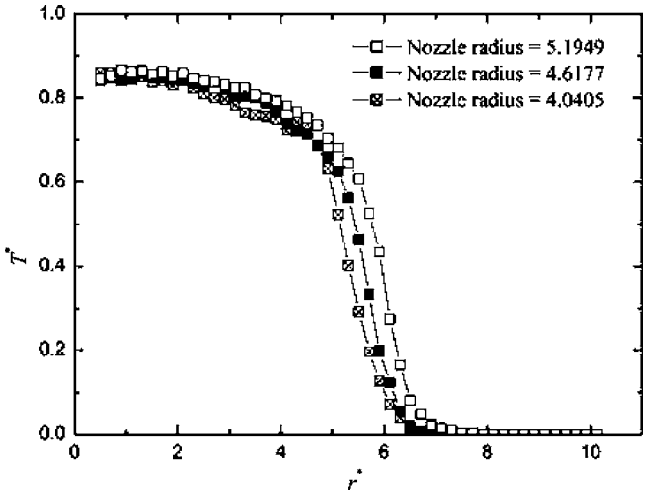

FIG. 8. Temperature variations along the radial direction r^* of the jet.

near the axis of the nozzle does not contain a large enough number of atoms to monitor the local temperature.

B. Comparison with linear instability theories

As shown in Figs. 2 and 3, the liquid nanojet results inherently in unstable motions due to the interfacial instability. The ejected jet becomes unstable against the surface tension forces during its evolution and finally breaks to form liquid droplets. Rayleigh [1] firstly considered the instability of an infinitely long liquid cylinder of radius r. Here we investigate the unstable motion of the liquid nanojet to determine whether the classical theories about jet instability still hold for a nanoscale system.

In the classical linear instability theory, the disturbance in the liquid jet produces a variation in the radius of the jet of wavelength λ and grows exponentially along the jet

$$a = a(0)\exp\left(\frac{\omega y}{v}\right), \tag{4}$$

where a denotes amplitude of disturbance, $a(0)$ initial amplitude of small magnitude, ω growth rate, v jet velocity, and y jet flow direction. According to Rayleigh, the instability of a uniform flow of inviscid incompressible liquid within the cylinder of radius r_0 is described as follows for Theory 1:

$$\omega = \left[\frac{\gamma}{\rho_{liq} r_0^3}\frac{I_n'(k')}{I_n(k')}k'(1-k'^2-n^2)\right]^{1/2}, \tag{5}$$

where ρ_{liq} denotes liquid density, I_n modified Bessel function of order n, k' dimensionless wave number, which is expressed as $k'=2\pi r_0/\lambda$, and I_n' the derivative of I_n with respect to k'. We regard the cylinder radius r_0 as the equimolar jet radius r_{eq}^*. The jet is unstable for $k'<1$ if $n=0$. In the macroscopic system, the most unstable mode or the fastest growing mode corresponds to a value of $k'=0.697$.

It should be pointed out that Eq. (5) or "Theory 1" is based on the assumption of inviscid liquid flow. When the effect of viscosity is taken into account, the jet shape and the instability might have different behaviors compared to the inviscid case. Chandrasekhar [2] solved the Navier-Stokes equation to study the effect of viscosity on the instability. When expanding his formula for small k' [4], we have for Theory 2,

$$\omega = \left(\frac{\gamma}{\rho_{liq} r_0^3}\right)^{1/2}\left\{\left[\frac{1}{2}k'^2(1-k'^2)+\frac{9}{4}\,\mathrm{Re}^{-2}k'^4\right]^{1/2} - \frac{3}{2}\,\mathrm{Re}^{-1}k'^2\right\}, \tag{6}$$

where Re is the Reynolds number. In the limit of small Reynolds numbers, Eq. (6) reduces to Theory 3

$$\omega = \frac{\gamma}{6 r_0 \eta_{liq}}(1-k'^2), \tag{7}$$

where η_{liq} is the liquid viscosity.

We have obtained a wide range of growth rates through numerical simulations for various nozzle radii and seed values. We have used Cline and Anthony's experimental method [12] in calculating the growth rate, that is, ω is expressed in terms of Z_0 and v as $\omega \sim v/Z_0$, where Z_0 is the uniform jet length, v the jet velocity, and Z_0/v the rupture time. Other investigators [3,13] experimentally measured the successive disturbance differences between the neck and the downstream neighboring swell in the jet to determine the growth rate. In this MD simulation, however, we cannot accurately measure the amplitude of growing disturbance. Since we did not directly impose a disturbance on the jet, we assumed that there were other disturbing factors inherent to liquid nanojets, and that the ratio of disturbance to jet radius was 0.05, the latter of which is consistent with an experimental study by Cline and Anthony [12]. Although we can choose this ratio to be different from 0.05, there is no change for the growth rate distribution shape. To estimate the growth rate, we should know the liquid properties, such as the surface tension, the viscosity, and the density. For the density, we have already shown its distribution in the jet in Fig. 5. We used the well-known Green-Kubo relation for the calculation of the viscosity of liquid argon. Bulk fluid is composed of 864 liquid atoms which interact with each other by the Lennard-Jones potential. We used the velocity scaling method to keep the temperature at $T_{jet}^*=0.8$. The MD simulation result gives $\eta_{liq}^*=2.23$, which is in close agreement with the result from the experimental correlation, $\eta_{exp}^*=2.10$ for liquid argon [14]. To determine the surface tension in the liquid-vapor interface, we used the calculation technique of Mecke *et al.* [11]. With a tail correction term and cutoff radius $r_c^*=5.0$, we obtained the surface tension of $\gamma^*=0.85$ at $T_{jet}^*=0.8$, which matches well with the result of Mecke *et al.*, $\gamma^*=0.86$.

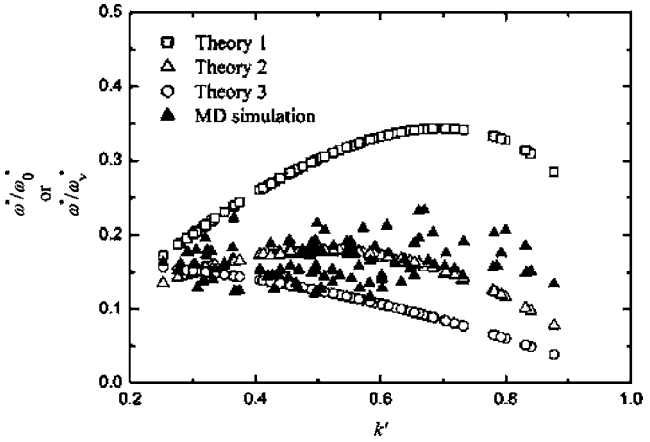

FIG. 9. Dimensionless growth rate of disturbance on the liquid nanojet. $\omega_0^*=(\gamma^*/\rho_{liq}^* r_0^{*3})^{1/2}$; $\omega_v^*=\gamma^*/r_0^*\eta_{liq}^*$.

Simulation results for the growth rate are shown and compared with the classical theories in Fig. 9. In this figure, the growth rate is presented in dimensionless form. For the same nozzle radius, we have obtained various magnitudes of the wave number using different seed values for extracting the initial velocities of atoms from the Maxwell-Boltzmann distribution. As expected, the inviscid theory (Theory 1) predicts the growth rate differently from the theory with the viscous effect included (Theory 2). In the case of Theory 3, which is the limiting case of an extremely high viscosity or a

very small Reynolds number, the growth rate slowly decreases with increasing wave number. For all simulation cases, the Reynolds number, which is defined as $\mathrm{Re}_{r_{eq}} = \rho_{liq} v_y r_{eq} / \eta_{liq}$, is fixed to be almost constant at the value of 2.17. As shown in Fig. 9, although MD simulation results for the growth rate show a distribution different from other classical instability theories, they are somewhat closer in magnitude to the results from Theory 2. The existence of numerical differences between Theory 2 and simulation data is mainly due to statistical uncertainties or thermal fluctuations. In the present study, it is found that the calculated dimensionless growth rate ω^* / ω_0^* ranges from 0.12 to 0.23 regardless of the wave number. From Fig. 9, we cannot determine easily where the fastest growing mode of nanojets exists. Nevertheless, previous works on the nanoscale liquid threads [5,6] have concluded that unstable motions can be well described by Theory 1 or Theory 3. It should be noted that their simulation results were limited to only five cases at the most. When a variety of initial conditions are used and the physical conditions such as density and temperature remain the same, we might not be able to confirm that the behaviors of the nanoscale liquid jet always follow the prediction of the classical theories. We can rather conclude that the magnitude of the simulation results is close to the classical prediction.

IV. CONCLUSION

The present paper is devoted to investigating the microscopic behaviors of a liquid jet using the molecular dynamics simulation with Lennard-Jones fluid. We have found various breakup motions of liquid nanojets depending on the nozzle radius and the initial velocity condition, which are very different from the estimates of continuum theories. Initial velocities of atoms, which are readily adjusted by the seed number, markedly influence the breakup length, the rupture time, the wavelength, and the formation of drops of the liquid nanojet. Detailed distributions of hydrodynamic properties, such as the liquid density, the streaming velocity and the temperature, are calculated across the nozzle using the slab method. Numerical results for a wide range of disturbance growth rates of a liquid nanojet are obtained and compared with those of the continuum-based theories. The MD simulation results are closer to Chandrasekhar's analysis than to Rayleigh's dispersion relation. With various simulation conditions, however, we cannot confirm that classical theories can be used to accurately predict the growth rate of the liquid nanojet. Instead simulation results show large local differences from the classical theories, mainly due to thermal fluctuations. The dimensionless growth rates tend to remain independent of the wave number. These conclusions suggest that the molecular dynamics simulation might be an alternative method for analyzing liquid nanojet behaviors where classical theories cannot be applied.

ACKNOWLEDGMENTS

This research was supported by Grant No. M102KN010010-05K1401-01010 from the Center for Nanoscale Mechatronics & Manufacturing of 21st Century Frontier Research Program of Korea.

[1] Lord Rayleigh, Philos. Mag. **34**, 145 (1892).
[2] S. Chandrasekhar, *Hydrodynamic and Hydromagnetic Stability* (Oxford University Press, Oxford, 1961).
[3] E. F. Goedde and M. C. Yuen, J. Fluid Mech. **40**, 495 (1970).
[4] J. Eggers, Rev. Mod. Phys. **69**, 865 (1997).
[5] J. Koplik and J. R. Banavar, Phys. Fluids A **5**, 521 (1993).
[6] S. Kawano, Phys. Rev. E **58**, 4468 (1998).
[7] M. Moseler and U. Landman, Science **289**, 1165 (2000).
[8] J. G. Powles, S. Murad, and P. V. Ravi, Chem. Phys. Lett. **188**, 21 (1992).
[9] G. Nagayama and P. Cheng, Int. J. Heat Mass Transfer **47**, 501 (2004).
[10] B. D. Todd, D. J. Evans, and P. J. Daivis, Phys. Rev. E **52**, 1627 (1995).
[11] M. Mecke, J. Winkelmann, and J. Fischer, J. Chem. Phys. **107**, 9264 (1997).
[12] H. E. Cline and T. R. Anthony, J. Appl. Phys. **49**, 3203 (1978).
[13] R. J. Donnelly and W. Glaberson, Proc. R. Soc. London, Ser. A **290**, 547 (1996).
[14] R. C. Reid, J. M. Prausnitz, and B. E. Polling, *The Properties of Gases and Liquids* (McGraw-Hill, New York, 1987).